Characterization and Application of Nanomaterials (2021) Volume 4 Issue 1
doi:10.24294/can.v4i1.523

ORIGINAL RESEARCH ARTICLE

Nano CoO-Cu-MgO catalyst for vapor phase simultaneous synthesis of *ortho*-chloroaniline and γ-butyrolactone from *ortho*-cholonitrobenzne and 1,4-butanediol

Hari Prasad Reddy Kannapu[1,2,3*], Young-Woong Suh[2,3*], Veeralakshmi Vaddeboina[1], Anand Narani[1], David Raju Burri[1], Seetha Rama Rao Kamaraju[1]

[1] *Catalysis, Indian Institute of Chemical Technology, Hyderabad 500007, India. E-mail: kannapuhari@gmail.com/ hari83@hanyang.ac.kr*

[2] *Department of Chemical Engineering, Hanyang University, Seoul 133-791, Republic of Korea. E-mail: ywsuh@hanyang.ac.kr*

[3] *Research Institute of Industrial Science, Hanyang University, Seoul 133-791, Republic of Korea*

ABSTRACT

The article aims at developing an efficient and stable catalysts for simultaneous hydrogenation of *o*-chloronitrobenzene to *o*-chloroaniline and 1,4-butanediol dehydrogenation to γ-butyrolactone. A series of CoO-Cu-MgO catalysts, composed of 10 wt% of copper, various amount of cobalt loadings (1, 5 and 10 wt%) and remaining of MgO were developed by co-precipitation followed by thermal treatment. *o*-Chloroaniline and γ-butyrolactone were the main products with high yield of 85% and 90%, respectively. The advantage of the coupling process is that the hydrogenation reaction was conducted without external hydrogen, demonstrating minimize the hydrogen consumption known as hydrogen economy route. From N_2O characterization results, the high activity of 5CoO-10Cu-MgO was found that it has high amount of Cu species (Cu^0/Cu^{+1}) which govern the stable activity and selectivity on time on stream study in presence of cobalt in Cu-MgO.

Keywords: Transfer Hydrogenation; *Ortho*-chloro Aniline; γ-Butyrolactone; Atomic H_2; Basic Sites; Nano CoO-Cu-MgO

ARTICLE INFO

Received: 13 November 2020
Accepted: 4 January 2021
Available online: 11 January 2021

1. Introduction

Owing to an enormous importance of aromatic halo amines in the chemical industry, specifically for synthesis of herbicides, dyes, drugs, and pesticides, synthesis of aromatic halo amines from halo nitrobenzene research has been gained a great attention in academia and industry point of view[1–9]. Despite high demanding of this reaction, the hydrogenation of *ortho*-chloronitrobenzene (*o*-CNB) to *ortho*-chloroaniline (*o*-CAN) has been studied extensively over precious metals e.g., platinum, palladium, nickel, rhodium, ruthenium and iridium[1–9]. Moreover, it has been mostly carried out under external hydrogen at an elevated temperatures and pressures which makes this process more complex and cost-ineffective in the industry point of view. Further, dehalogenation and ring hydrogenation are common side reactions that lead to formation of common side reactions that lead to formation of aniline and cyclohexylamine particularly over Pt, Pd and Ni catalysts. In this scenario, developing a highly selective and cost-effective cat-

alytic system still remains a challenge. Generally, alcohols are highly active for dehydrogenation over supported copper catalysts[10–18]. 1,4-butanediol (BDO) is one of the alcohols that can make γ-butyrolactone (GBL) and two moles of hydrogen in its cyclodehydrogenation over copper-based catalysts. Another important point is noticed that the GBL has been demonstrated to be involved in the synthesis of N-vinylpyrrolidone, N-methylpyrrolidone, herbicides, and rubber additives and more over it is a green solvent. Commercially, the major production route for GBL is gas-phase dehydrogenation of BDO over supported copper metal catalysts, especially copper chromite catalysts, which are environmentally unacceptable.

As described above, owing to the high commercial value of these products, these two reactions would have great impression. Currently, coupling of hydrogenation and dehydrogenation[10–17] is a promising and an alternative method to the conventional hydrogenation. In this method, the above mentioned two reactions can be carried out simultaneously at a time over a same catalyst bed. Copper-based catalysts were found to be outstanding for the coupling of hydrogenation and dehydrogenation reaction[10–16]. However, the activity and stability of catalysts mainly depends on the preparation of the catalysts. A numerous results documented in the literature have found that the addition of second metal oxide to base catalyst will result in the local composition, the size and structure of active species significantly affecting the catalytic activity and selectivity of supported metal catalysts[19]. It is generally agreed that for supported metal catalysts, highly dispersed active species can provide more active sites and thus confer the resulting catalysts with higher catalytic activity[20]. To best of our knowledge, selective *o*-CNB hydrogenation to *o*-CAN has not been reported using 1,4-butanediol (BDO) dehydrogenation over nano CoO-Cu-MgO.

Herein, we have investigated the vapor phase selective hydrogenation of *o*-CNB to *o*-CAN with dehydrogenation of BDO to γ-butyrolactone (GBL) over CoO-Cu-MgO catalysts. All the catalysts were developed by co-precipitation followed by thermal treatment. Catalysts preparation, characterization using different analytical techniques such as BET surface area, N_2O pulse chemisorption, XRD, TPR-H_2, and TEM analysis and activity in hydrogenation and dehydrogenation have been delineated.

2. Experimental

2.1 Preparation of catalysts

An aqueous homogeneous mixed metal nitrate solution containing $Cu(NO_3)_2$•$3H_2O$ and $Mg(NO_3)_2$•$6H_2O$ was prepared followed immediate precipitation by drop-wise addition of 10% aqueous K_2CO_3 solution at a pH of 9.0 under constant stirring at room temperature. The resultant mixed Cu-Mg precipitate (precipitate of 10 wt% Cu-MgO catalyst, ppt1) has been separated under reduced pressure and washed thoroughly with hot distilled H_2O until the complete removal of potassium ion. In a separate experiment, requisite amount of $Co(NO_3)_2$•$6H_2O$ aqueous solution has been precipitated at a pH of 9 with K_2CO_3 solution under vigorous stirring. The obtained cobalt precipitate (ppt2) was filtered and washed thoroughly with hot distilled water. Cu-Mg precipitate (ppt1) and Co precipitate (ppt2) were mixed in water under neutral condition and the resultant slurry was subjected to hydrothermal treatment at 373 K for 12 h followed by filtration with repeated washings. The precipitate was dried in oven at 393 K for 12 h followed by calcination at 723 K for 5 h. Similar procedure has been adopted for the preparation of other CoO promoted Cu-MgO catalysts. The prepared catalysts were labeled as 1CoO-10Cu-MgO, 5CoO-10Cu-MgO, and 10CoO-10Cu-MgO, here the numerical value represents the loadings of Co and Cu by weight percentage. For example, 1CoO-10Cu-MgO represents a catalyst containing 1 wt% Co, 10 wt% Cu and the remaining balance MgO.

2.2 Characterization techniques

All the CoO-Cu-MgO catalysts were thoroughly characterized by using the following analytical techniques. The Brunauer, Emmett and Teller (BET) surface area of all catalysts was measured by N_2 physisorption after degasification at 473 K for 4 h, under liquid nitrogen adsorption at 77 K using

Quadrasorb-SI surface area analyzer (M/s. Quantachrome instruments, USA). The surface properties of all CoO-Cu-MgO catalysts such as Cu metal surface area (MSA), Cu dispersion (D_{Cu}), particle size (P_{Cu}) and surface coverage of Cu atoms (S_{Cu}) were estimated by N_2O pulse chemisorption on pre-reduced (553 K for 3 h) catalyst under dynamic conditions. The detailed procedure was described elsewhere[10–13]. The X-ray diffraction (XRD) patterns of both calcined and reduced catalysts were recorded on a Miniflex diffractometer (M/s. Rigaku Instruments, Japan) using Ni filtered Cu K_α radiation in the 2θ range of 10°–80° at a scan rate of 2° min^{-1}. The average crystallite size of copper was calculated using Debye-Scherrer principle. Transmission electron microscopy (TEM) was recorded using a Phillips Tecnai G2 FEI F12 electron microscope. The reduction behavior of the catalysts was determined by temperature programmed reduction (TPR) studies on a home-made system as per the procedure described elsewhere[10]. The CHNS elemental analysis was carried out on Elementar, Model: VarioMicrocube to estimate the carbon content in the catalyst before and after the reaction.

2.3 Activity studies

A down flow fixed-bed reactor was used to investigate the activity of the CoO-Cu-MgO catalysts for the individual hydrogenation of *o*-CNB (dissolved in ethanol) to *o*-CAN and dehydrogenation of BDO to GBL as well as coupling of both reactions. For separate experiments, first tests were carried out on *o*-CNB hydrogenation. Approximately, 500 mg of the catalyst powder (sieved to < 200 μm) diluted with an equal amount of quartz beads was charged to the reactor and supported on a quartz wool bed. The catalyst was reduced at 553 K for 3 h under hydrogen. Then, the reactor was fed with *o*-CNB under H_2 (18 ml·min^{-1}), using as a reducing gas. Similarly, the dehydrogenation of BDO was conducted under N_2 atmosphere. Finally, the coupling of *o*-CNB hydrogenation and BDO dehydrogenation was performed at the molar ratio of 2:3 under nitrogen atmosphere. The liquid products, such as *o*-CAN and GBL were analyzed by using GC-17A (M/s. Shimadzu, Japan) with ZB-wax capillary column equipped FID detector. The products were identified and analyzed by using GCMS–QP5050 (M/s. Shimadzu instruments, Japan) equipped with ZB-5 capillary column (25 m × 0.32 mm) supplied by M/s. J&W Scientific, USA.

3. Results and discussion

3.1 Catalyst characterization

3.1.1 BET Surface area studies

Table 1 presents BET surface area, crystalline phases of various cobalt loadings of Cu-MgO catalysts both in calcined and reduced form. The surface area of the CoO-Cu-MgO catalysts is higher compared to MgO (42 $m^2 \cdot g^{-1}$) alone. This indicates that addition of cobalt to Cu-MgO increases the surface areas of Cu-MgO.

The BET surface area of catalysts increases with increasing in CoO loading and displayed maximum surface area (88 $m^2 \cdot g^{-1}$) at 5 wt% CoO loading and thereafter decreases with further increasing in the Co content. It was found that hydrothermal treatments of Fe/MgO catalysts transformed into lamella-like Fe/$Mg(OH)_2$ catalysts, resulted in increasing the specific surface areas[21]. Since, in the present study, due to hydrothermal treatment, CoO-CuO-MgO interacted species in large number is responsible for high surface area of 5CoO-10Cu-MgO catalyst. Formation of an interacted phase ($CuCo_3O_4$) between Cu and Co was reported to be appeared at a temperature of 573 K which was stable up to 1073 K[22]. Such interacted phase might be accountable for the increasing trend of surface area and pore volume with the increase in Co content up to 5 wt%. Contrarily, beyond 5 wt%

Table 1. BET surface area and XRD results of CoO-Cu-MgO catalysts

Catalyst	BET surface area ($m^2 \cdot g^{-1}$)	XRD phases		Cu^0 (nm) reduced	Cu^0 (nm) spent
		Calcined	Reduced		
1CoO-10Cu-MgO	78	CuO, MgO	Cu^0, Cu_2O,MgO	20	30.48
5Co-10Cu-MgO	88	CuO, MgO	Cu^0, Cu_2O,MgO	15	20.30
10CoO-10Cu-MgO	50	CuO, MgO	Cu^0, Cu_2O,MgO	13	26.48

Co loading, a reverse trend was observed due to surface coverage by cobalt oxide. The crystallite size of copper in reduced and spent catalysts is calculated and depicted in **Table 1**. It is obvious that the development of copper size influenced by the cobalt addition is inevitable. In the case of reduced catalysts copper crystallite size linearly minimized whereas in spent catalysts, only 5CoO-10Cu-MgO has stability and maintain lower crystallite size among other two catalysts.

3.1.2 X-Ray diffraction studies (XRD)

The XRD patterns of calcined catalysts are shown in **Figure 1**. A low intense diffractions of CuO phase (d values of 2.52 at 2θ = 35.6°, 2.32 at 2θ = 38.78 and 2.53 at 2θ = 35.45°, ICDD Card No. 5-661) and high intensity of MgO (d values of 2.11 at 2θ = 42.82°, 1.49 at 2θ = 62.25° and 1.22 at 2θ = 78.30°, ASTM Card No. 4-829) are observed in all cobalt loading catalysts. Interestingly, no diffractions were noticed for CoO oxide phase at all loadings which indicates amorphous form of cobalt species. It was reported that in 11% Co-MgO catalyst, MgO is in amorphous form when it is calcined at 673 K and it is in crystalline phase above 973 K[23]. In addition, CoO is formed after calcination at 773 K through the decomposition of $Co(NO_3)_2$ and might have diffused into the matrix of MgO or form a solid solution or oxidized to Co_2O_3, which on reaction either with CoO or with MgO to yield Co_3O_4 or $MgCo_2O_4$[24].

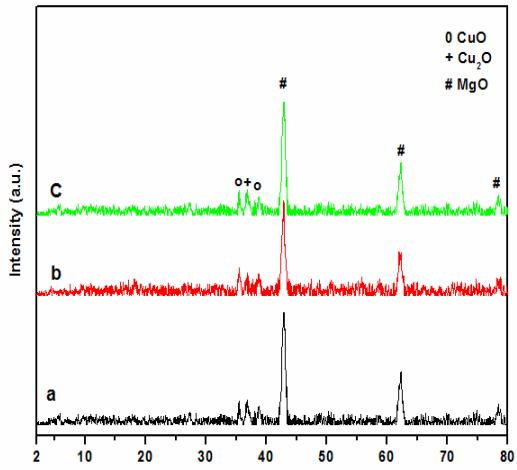

Figure 1. XRD patterns of calcined CoO-Cu-MgO catalysts. **(a)** 1CoO-10Cu-MgO; **(b)** 5CoO-10Cu-MgO; **(c)** 10CoO-10Cu-MgO.

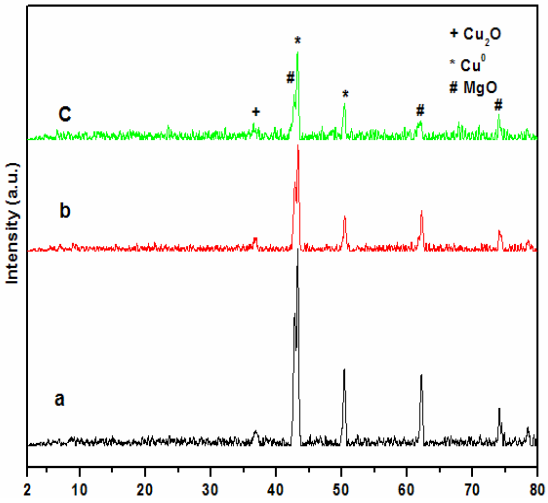

Figure 2. XRD patterns of reduced CoO-Cu-MgO catalysts. **(a)** 1CoO-10Cu-MgO; **(b)** 5CoO-10Cu-MgO; **(c)** 10CoO-10Cu-MgO.

XRD patterns of reduced (at 523 K in H_2 flow) CoO-Cu-MgO catalysts are shown in **Figure 2**. The Cu^0 phase with corresponding d values of 2.09 at 2θ = 43.25°, 1.81 at 2θ = 50.37° and 1.28 at 2θ= 73.99°, ICDD Card No. 4-836 is observed for all catalysts. But, the d values of Cu^0 and MgO are closer; therefore, the diffraction lines are not separated properly. As evidenced from the XRD results almost all CuO phases are reduced to Cu^0 or Cu_2O. It can also be seen that MgO phase decreased with addition of cobalt oxide representing the formation of amorphous $MgCo_2O_4$ species particularly at 10 wt% CoO. XRD pattern of 10CoO-10Cu-MgO catalyst revealed that Cu^0, Cu_2O and MgO crystallites were lower than other two catalysts.

3.1.3 N_2O pulse chemisorption

The estimated surface properties of Cu-MgO with cobalt catalysts such as (i) number of surface copper sites, (ii) dispersion, (iii) metal surface area, and (iv) particle size are shown in **Table 2**. N_2O pulse chemisorption is a facile and proven technique for the estimation of metal area and allied surface properties of supported copper catalysts.

Even though Co oxides are hard to get reduced at 523 K (the temperature at which the catalysts of the present investigation are reduced prior to N_2O pulse chemisorption), small amount of lower oxidation states of Co species might have resulted to participate in the decomposition of N_2O thus giving

Table 2. N_2O pulse chemisorption results for different CoO-10Cu-MgO catalysts

Catalyst	S_{Cu} atoms × 10^{-19} (atoms g^{-1})	D_{Cu} (%)	Metal surface area ($m^2 \cdot g^{-1}$)	Particle size (nm)	Surface density S_{Cu}/BET S.A
1CoO-10Cu-MgO	10	19	07	13	10/78
5CoO-10Cu-MgO	18	21	13	06	18/88
10CoO-10Cu-MgO	12	14	11	10	12/50

Note: S_{metal} = Number of surface metal sites (Cu); D_{metal} = Dispersion of metal (Cu); SA_{metal} = Surface area of metal (Cu); P_{metal} = Particle size of metal (Cu)

a chance to over estimation of Cu dispersion[12]. As shown in **Table 2**, the number active surface sites of copper catalysts are higher in 5CoO-10Cu-MgO. Similarly, dispersion of active metal (copper plus cobalt) and active metal surface area (copper plus cobalt) are higher in all the cobalt promoted catalysts. Contrarily, the particle size (copper plus cobalt) of metal is lower in all cobalt promoted catalysts. 5CoO-10Cu-MgO catalyst possesses a little higher surface density (copper plus cobalt) compared to other Co promoted catalysts. The surface density of 5CoO-10Cu-MgO catalyst is nearly double than that of 1CoO-10Cu-MgO catalyst.

3.1.4 TEM analysis

Figures 3a, **b** and **c** are copper particles with an appearance of dark contrasts as well as copper-free MgO particles with an appearance of light contrasts. At lower cobalt loadings the morphology of catalysts seems to be rod type structure, whereas at 10CoO-10Cu-MgO, catalyst regains its particle type structure. Such a gathering of copper species in CoO-Cu-MgO catalysts has also been reported in the literature[21–25]. However, no obvious copper particles can be found in the hydrothermal-treated catalyst (**Figure 4**).

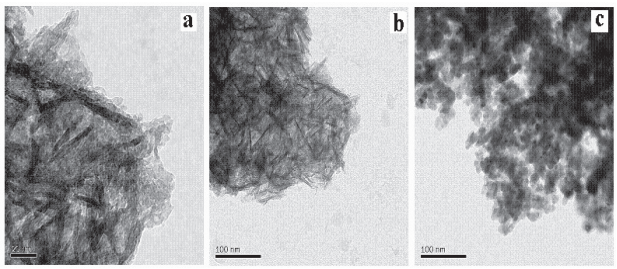

Figure 3. TEM images of CoO-Cu-MgO. **(a)** 1CoO-10Cu-MgO; **(b)** 5CoO-10Cu-MgO; **(c)** 10CoO-10Cu-MgO.

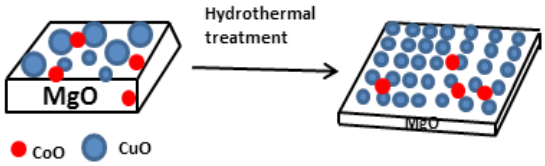

Figure 4. Suggested mechanism of hydrothermal treatment and nanoparticle growth.

3.1.5 Temperature programmed reduction (TPR) studies

The reducibility of the catalysts can be determined by temperature programmed reduction with H_2/Ar mixture and results are depicted in **Figure 5**. According to the TPR results of 10Cu-MgO catalyst, the catalyst characterized by a single symmetric peak centered at a temperature maximum (T_m) of 710 K[16]. The present results showed that the 1CoO-10Cu-MgO catalyst exhibits a single reduction, indicating the 1 wt% CoO did not affect Cu-MgO interactions. However, presence of a shoulder on an asymmetric peak is the indication of two-stage reduction: (i) CuO to Cu^0 and (ii) partial reduction of $CuCo_2O_4$/$MgCo_2O_4$. In the case of 5CoO-10Cu-MgO catalyst, the high temperature signal corresponds to the reduction of interacted species formed between CoO precursor and CuO. It is noteworthy to mention that the amount of cobalt oxide species are less at 5 wt% cobalt oxide compared with that of 10 wt% CoO. The reaction between CuO and CoO can make more $CuCO_2O_4$ species in 5CoO-10Cu-MgO. Whereas, the high cobalt oxide content in 10CoO-10Cu-MgO might have resulted to have less $CuCO_2O_4$ and more $MgCo_2O_4$ which are reduced at 850 K. The three-stage reduction including copper oxide, cobalt oxides and spinals ($CuCO_2O_4$ and $MgCO_2O_4$) providing high acidity for 10CoO-10Cu-MgO.

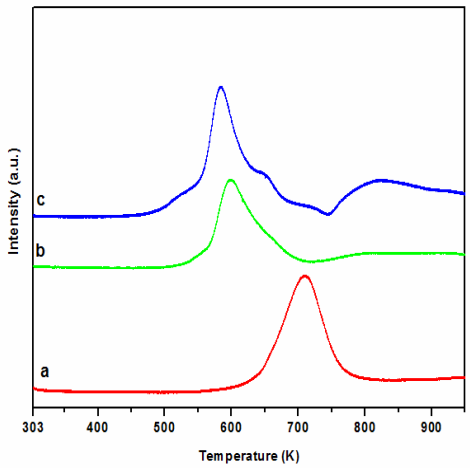

Figure 5. TPR patterns of CoO-Cu-MgO. **(a)** 1CoO-10Cu-MgO; **(b)** 5CoO-10Cu-MgO; **(c)** 10CoO-10Cu-MgO.

Due to high cobalt oxide content in 10CoO-10Cu-MgO, the reduction behavior is unlike to other two catalysts. It was reported that the peaks at 650 and 730 K were assigned to reduction of large crystalline Co_3O_4 to CoO and CoO to Co metal, respectively, but a shoulder peak at 850 K was attributed to the reduction of $MgCo_2O_4$[26]. As reported by Wang and Ruckenstein[24], Co_3O_4 is getting reduced below 773 K while $MgCo_2O_4$ below 973 K and the solid solution of Co-MgO at higher than 1273 K temperature. The TPR results of this study are well collaborated with those reported in the literature[12]. The shifting of T_{max} to lower temperature in 5 wt% and 10 wt% Co catalysts is an indication of interaction between Co and Cu species. It was reported that when a mixture of Cu and Co oxides were supported on Al_2O_3, cobalt oxide reacts during calcination not only with CuO but also with Al_2O_3, which leads to formation of the spinel $CoAl_2O_4$[27]. When the same oxides were supported on non-interacted supports like silica, they interact to form the spinel $Cu-Co_2O_4$[28]. Thus, the TPR patterns clearly indicate the presence of Co oxide interacted species with both Cu and Mg-oxides.

3.2 Activity studies

3.2.1 Hydrogenation of *ortho*-chloronitrobenzene (*o*-CNB)

The catalytic activity of CoO-Cu-MgO catalysts evaluated for the vapor phase selective hydrogenation of *o*-CNB to *o*-CAN at atmospheric pressure with H_2/*o*-CNB required mole ratio at a reaction temperature in the range of 548 K–723 K and results are shown in **Figure 6**. The conversion of *o*-CNB to *o*-CAN increases significantly with the increasing of temperature from 540 K to 680 K. Thereafter conversion is nearly about 95% and 90% for 5CoO-10Cu-MgO and 1CoO-10Cu-MgO, respectively. Precisely, 5CoO-10Cu-MgO has shown highest conversion about 98% at 720 K. But, the conversion of *o*-CNB to *o*-CAN is maximum of 63% at 673 K and reached to 50% at final temperatures over 10CoO-10Cu-MgO. These results demonstrated the effect of cobalt loadings on hydrogenation of *o*-CNB to *o*-CAN over CoO-Cu-MgO. The high activity of 5CoO-10Cu-MgO is associated to the presence of more number of surface active Cu^0 particles as observed from N_2O pulse chemisorption.

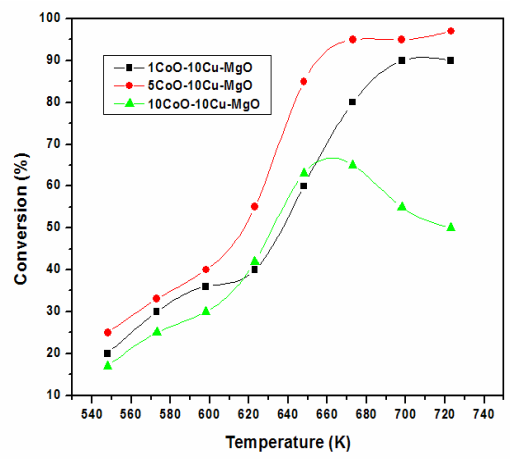

Figure 6. Effect of temperature on hydrogenation of *ortho*-chloronitrobenzene over CoO-Cu-MgO catalysts.

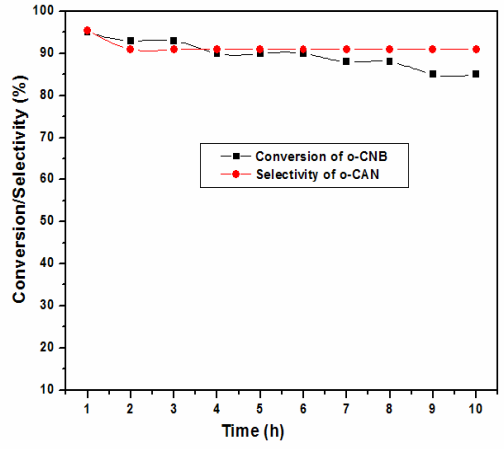

Figure 7. Time on studies over 5CoO-10Cu-MgO at 623 K for 10 h.

Figure 7 shows the conversion of *o*-CNB to *o*-CAN at 623 K over a period of 10 h reaction. It is found that the activity of the catalyst is stable with 90% conversion up to 6 h and then reached to 85% at final hours. It is concluded that agglomeration of copper might responsible for loss of the activity. These results are good agreement with that the crystallite size of copper after reaction is bigger than reduced copper as shown in **Table 1**.

3.2.2 Dehydrogenation of 1,4-butanediol (BDO)

Figure 8 illustrates BDO conversion as a function of temperature. The dehydrogenation of BDO is an endothermic reaction; hence the conversion of BDO to GBL increases with the rise of temperature over CoO-Cu-MgO catalysts. The result shows that the maximum catalytic activity of CoO-Cu-MgO catalysts is noticed at 523 K, which is best temperature to obtain the GBL with high yields. In contrast, conversion of BDO is falling gradually for all catalysts except over 5CoO-Cu-MgO. The highest BDO conversion (> 97%) and GBL selectivity (99%) can be seen at 5 wt% CoO loading Cu-MgO. Importantly, the selectivity towards GBL is all most same for all the catalysts.

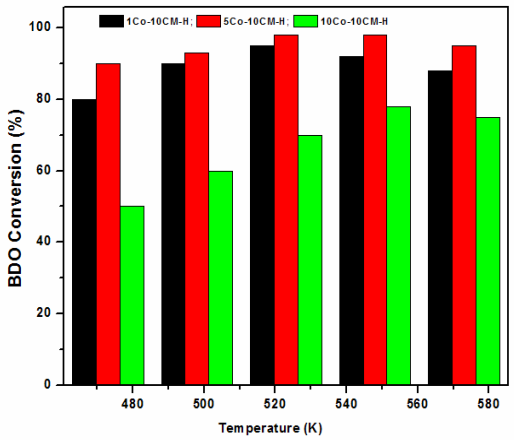

Figure 8. Effect of temperature on BDO dehydrogenation over CoO-Cu-MgO catalysts.

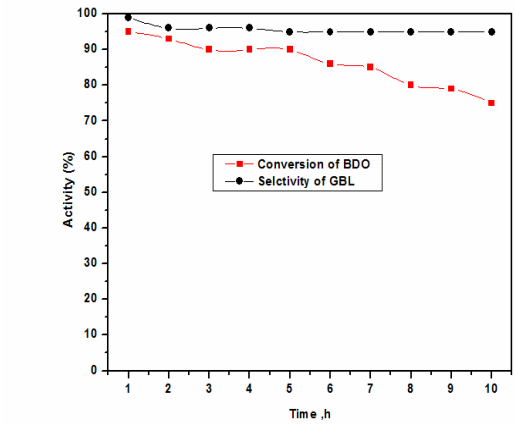

Figure 9. Time on stream study of BDO dehydrogenation over 5Co-10CM-H catalyst.

Based on above results, the stability of 5CoO-10Cu-MgO for BDO to GBL was evaluated for 10 h at 523 K. The conversion of BDO is above 95% at beginning of the reaction whereas with increasing in the time the conversion declines slowly from 95% to 75%. Interestingly, selectivity to GBL remains constant up to 10 h (**Figure 9**). The deactivation of the catalyst is mainly due to agglomeration of copper particles during course of the reaction.

3.2.3 Coupling of *o*-chloronitrobenzene hydrogenation and 1,4-butanediol dehydrogenation

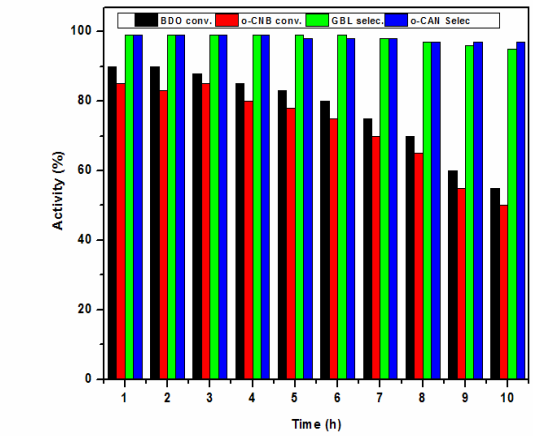

Figure 10. Time on stream study coupling of BDO dehydrogenation and *o*-CNB hydrogenation over 5Co-10CM-H catalyst.

The independent reactions: (i) hydrogenation of *o*-CNB to *o*-CAN and (ii) dehydrogenation of BDO to GBL provide the best catalyst and temperature to conduct the titled reactions. The mole ratio of BDO

versus *o*-CNB is 1.5:1, which is an optimum for coupling process and results are shown in **Figure 10**. The reaction results clearly demonstrate that conversions of BDO and *o*-CNB are 90% and 85%, respectively, in early hours. When reaction time increases, the conversion of both reactions linearly dropped which could be attributed to the agglomeration of copper and finally reached to 54% and 50% with 99% selectivity of their corresponding products. Surprisingly, the individual hydrogenation of *o*-CNB at 523 K with 1.5 moles of external hydrogen is very low (< 5%). But, in coupling process, hydrogenation of *o*-CNB with dehydrogenation of BDO was substantially increased from 5% to 90%. This enhancement of *o*-CNB conversion in the coupling reaction is ascribed to the active role of in-situ production of hydrogen atom from BDO to GBL reaction which gets instantaneously utilized[10–18]. The deactivation of catalysts may be due to agglomeration copper. The color of the catalyst physically changed to black, which further indicates the coke deposition on the catalyst during course of the reaction.

4. Conclusions

The different amount of CoO incorporated 10Cu-MgO prepared by co-precipitation followed by hydrothermal treatment has shown excellent catalytic activity compared to unpromoted Cu-MgO catalyst. The best catalytic activity of 5Co-10Cu-MgO is due to the addition of cobalt increased number of surface copper atoms and decreased the reduction ability of copper as observed from TPR results. Contrarily, in 10CoO-10Cu-MgO the high amount of cobalt oxide covered active copper sites. Deactivation of catalyst in coupling reaction is mainly due to agglomeration as well the coke formation during the course of reaction. In summary, two industrially important reactions can be carried out over CoO-Cu-MgO catalyst simultaneously.

Conflict of interest

The authors declare that they have no conflict of interest.

Acknowledgements

Authors gratefully thank CSIR-UGC (INDIA) for the financial support. This research was also financially supported by Basic Science Research Program through the National Research Foundation of Korea (NRF) funded by the Ministry of Education (NRF-2016R1A6A1A03013422) and New & Renewable Energy Core Technology Program of the Korea Institute of Energy Technology Evaluation and Planning (KETEP), granted financial resource from the Ministry of Trade, Industry & Energy, Republic of Korea (No. 20163010092210).

References

1. Yang X, Deng Z, Liu H. Modification of metal complex on hydrogenation of *ortho*-chloronitrobenzene over polymer-stabilized platinum colloidal clusters. Journal of Molecular Catalysis A: Chemical 1999; 144: 123.
2. Khilnani VL, Chandalia SB. Selective hydrogenation. I. para-chloronitrobenzene to para-chloroaniline platinum on carbon as catalyst. Organic Process Research and Development 2001; 5: 257.
3. Liang M, Wang X, Liu H, *et al.* Excellent catalytic properties over nanocomposite catalysts for selective hydrogenation of halonitrobenzenes. Journal of Catalysis 2008; 255: 335.
4. Motoyama Y, Kamo K, Nagashima H. Catalysis in polysiloxane gels: Platinum-catalyzed hydrosilylation of polymethyl hydrosiloxane leading to reusable catalysts for reduction of nitroarenes. Organic Letter 2009; 11: 1345.
5. Yuan X, Yan N, Xiao C, *et al.* Highly selective hydrogenation of aromatic chloronitro compounds to aromatic chloroamines with ionic-liquid-like copolymer stabilized platinum nano catalysts in ionic liquids. Green Chemistry 2010; 12: 228.
6. Yang X, Liu H, Zhong H. Hydrogenation of ortho-chloronitrobenzene over polymer-stabilized palladium–platinum bimetallic colloidal clusters. Journal of Molecular Catalysis A: Chemical 1999; 147: 55.
7. Sreedhar B, Reddy PS, Devi DK. Direct one-pot

reductive amination of aldehydes with nitroarenes in a domino fashion: Catalysis by gum-acacia-stabilized palladium nanoparticles. Journal of Organic Chemistry 2009; 74: 8806.
8. Liu M, Yu W, Liu H. Selective hydrogenation of ortho-chloronitrobenzene over polymer-stabilized ruthenium colloidal catalysts. Journal of Molecular Catalysis A: Chemical 1999; 138: 295.
9. Kratky V, Kralik M, Mecarova M, *et al.* Effect of catalyst and substituents on the hydrogenation of chloronitrobenzenes. Applied Catalysis A 2002; 235: 225.
10. Nagaraja BM, Padmasri AH, Seetharamulu P, *et al.* A highly active Cu-MgO-Cr_2O_3 catalyst for simultaneous synthesis of furfuryl alcohol and cyclohexanone by a novel coupling route—Combination of furfural hydrogenation and cyclohexanol dehydrogenation. Journal of Molecular Catalysis A: Chemical 2007; 278: 29.
11. Reddy KHP, Mullen CA, Elkasabi Y, *et al.* Catalytic transfer hydrogenation for stabilization of bio-oil oxygenates: Reduction of p-cresol and furfural over bimetallic Ni–Cu catalysts using isopropanol. Fuel Processing Technology 2015; 137: 220–228.
12. Reddy KHP, Neeli CKP, Rao KSR, *et al.* Unusual effect of cobalt on Cu–MgO catalyst for the synthesis of γ-butyrolactone and aniline *via* coupling reaction. Catalysis Science and Technology 2016; 6: 5494.
13. Reddy KHP, Rahul R, Reddy SSV, *et al.* Coupling of 1,4-butanediol dehydrogenation reaction with the hydrogenation of nitrobenzene over Cu/MgO catalysts. Catalysis Communication 2009; 10: 879.
14. Reddy KHP, Anand N, Venkateswarlu V, *et al.* A selective synthesis of 1-phenylethanol and γ-butyrolactone through coupling processes over Cu/MgO catalysts. Journal of Molecular Catalysis A: Chemical 2012; 355: 180.
15. Reddy KHP, Suh YW, Anand N, *et al.* Coupling of 1,4-butanediol dehydrogenation with nitrobenzene hydrogenation for simultaneous synthesis of γ-butyrolactone and aniline over promoted Cu-MgO catalysts: Effect of promoters. Catalysis Letters 2017; 147: 90–101.
16. Reddy KHP, Young-Woong S, Anand N, *et al.* Coupling of *ortho*-chloronitrobenzene hydrogenation with 1,4-butanediol dehydrogenation over Cu-MgO catalysts: A hydrogen free process. Catalysis Communications 2017; 95: 21–25.
17. Reddy KHP, Young-Woong S, Anand N, *et al.* One-pot synthesis of ethylbenzene/1-phenylethanol and γ-butyrolactone from simultaneous acetophenone hydrogenation and 1,4-butanediol dehydrogenation over copper based catalysts: Effect of support. RSC Advances 2017; 7: 35346–35356.
18. Reddy KHP, Anand N, PSS Prasad, *et al.* Influence of method of preparation Co-Cu-MgO catalysts on dehydrogenation/dehydration reaction pathway of 1,4-butanediol. Catalysis Communications 2011; 12: 866–869.
19. Daage M, Chianelli RR. Structure-function relations in molybdenum sulfide catalysts: The "rim-edge" model. Journal of Catalysis 1994; 149: 414.
20. Vradman L, Landau MV, Herskowitz M, *et al.* High loading of short WS2 slabs inside SBA-15: Promotion with nickel and performance in hydrodesulfurization and hydrogenation. Journal of Catalysis 2003; 213: 163.
21. Ning G, Liu Y, Wei F, *et al.* Porous and lamella-like Fe/MgO catalysts prepared under hydrothermal conditions for high-yield synthesis of double-walled carbon nanotubes. Journal of Physical Chemistry C 2007; 11: 1969.
22. Shaheen WM, Ali AA. Characterization of solid–solid interactions and physicochemical properties of copper-cobalt mixed oxides and $Cu_xCo_{3-x}O_4$ spinels. Materials Research Bulletin 2001; 36: 1703.
23. Omata K, Nukui N, Hottai T, *et al.* Cobalt-magnesia catalyst by oxalate co-precipitation method for dry reforming of methane under pressure. Catalysis communications 2004; 5: 771.
24. Wang H, Ruckenstein E. CO_2 reforming of CH_4 over Co/MgO solid solution catalysts effect of calcination temperature and Co loading. Applied Catalysis A: General 2001; 209: 207.
25. Ago H, Nakamura K, Uehara N, *et al.* Roles of metal−support interaction in growth of single- and double-walled carbon nanotubes studied with diameter-controlled iron particles supported on MgO. Journal of Physical Chemistry B 2004; 108: 18908.
26. Furusawa T, Tsutsumi A. Comparison of Co/MgO

and Ni/MgO catalysts for the steam reforming of naphthalene as a model compound of tar derived from biomass gasification. Applied Catalysis A: General 2005; 278: 207.
27. Stoyanova D, Christova M, Dimitrova P, *et al.* Copper–cobalt oxide spinel supported on high-temperature aluminosilicate carriers as catalyst for $CO–O_2$ and CO–NO reactions. Applied Catalysis B 1998; 17: 233.
28. Cesar DV, Perez CA, Schmal M, *et al.* Quantitative XPS analysis of silica-supported Cu–Co oxides. Applied Surface Science 2000; 157: 159.